Bull. Mater. Sci., Vol. 39, No. 6, October 2016, pp. 1603–1608. © Indian Academy of Sciences.
DOI 10.1007/s12034-016-1292-x

Electrochemical properties of dip-coated vanadium pentaoxide thin films

R S INGOLE and B J LOKHANDE*
School of Physical Sciences, Solapur University, Solapur 413 255, India

MS received 6 August 2015; accepted 4 April 2016

Abstract. **Vanadium oxide (V_2O_5) thin films have been deposited on to the stainless-steel substrates by simple dip-coating technique using vanadium pentaoxide as an initial ingredient. Deposited samples were annealed at 773 K for 3 h in air. X-ray diffraction analysis of the sample shows crystalline with orthorhombic crystal structure. Scanning electron microscopy study depicts the homogeneous and dense surface morphology. Optical study proves the direct bandgap transition with energy ∼2.25 eV. Electrochemical performance of the deposited electrode was studied in 1 M $NaNO_3$ electrolyte using cyclic voltammetery, electrochemical impedance spectroscopy and galvanostatic charge–discharge tests. Prepared V_2O_5 electrode shows 207.50 F g^{-1} specific capacitance at the scan rate 5 mV s^{-1}, specific energy, specific power and efficiency are 41.33 Wh kg^{-1}, 21 kW kg^{-1} and 96.72%, respectively. The internal resistance observed from impedance spectroscopy is ∼8.77 ohm. Electrode exhibits excellent chemical stability up to 1000 cycles.**

Keywords. **Chemical synthesis; annealing; thin films; electrochemical properties; energy storage.**

1. Introduction

Supercapacitors or electrochemical capacitors (ECs) are investigated as potential energy storage elucidations because of high energy density than conventional capacitors and high power density than batteries [1,2]. Supercapacitor types are based on Helmholtz's double-layer capacitance, which is formed on an electrode/electrolyte interface (EDLC), and a pseudocapacitance, which results from a fast reversible faradic process, redox active materials, e.g., transition metal oxides or conducting polymers [3,4]. Because of the combined features of conventional capacitor and batteries, it has lot of commercial applications in several fields; such as, hybrid electric vehicles, laser, fuel cells, cellular phones, digital camera, etc. [5]. In the preparations of supercapacitor electrodes, transition metal oxides, conducting polymers and activated carbon materials are preferably used via different techniques [6–12]. Among these, transition metal oxides specially offer low electrochemical series resistance (ESR), more valance states, long cycle life, porous nature, etc. Some of the most extensively studied transition metal oxides for ECs are hydrous ruthenium oxide [13], iridium oxide [14,15], vanadium oxide [16,17], chromium oxide [18,19], etc. Contrarily, their high costs forced scientists to look for the cheap alternatives.

In this regard, cheap and abundantly available vanadium oxide is one of the promising electrode material because of large potential window, multivalences, high redox activity, 3D architecture and large stability [20]. Vanadium oxide and their compounds have attracted much attention for their important applications in various fields, such as lithium batteries [21–24], actuators [25], sensors [26], catalysis [27], optical switching devices [28] and electrochemical supercapacitors [29–31]. Vanadium oxide (V_2O_5) is found to be a promising electrode material of suitable layered crystal structures to get high-specific capacitance [32,33].

However, these applications depend on the techniques used to grow the films and the performance of the films is linked to its crystallinity and morphology [34]. V_2O_5 films have been prepared by various techniques, such as sol–gel deposition [35], vacuum evaporation [36], sputtering [37], electron-beam evaporation [38], spray pyrolysis technique [39] and dip coating [40]. Dip coating is one of the most widely used methods for depositing metal oxides onto large surfaces and cylinder- or irregular-shaped objects [41], where the substrate is first immersed into and subsequently extracted from a precursor solution (suspension), thus resulting as thin films on the surface of substrate. This method also offers certain advantages over conventional deposition techniques like simplicity, versatility, cost effectiveness, processing temperatures, quantity of product, control of stoichiometry and film structure etc. Stainless-steel (SS) substrates that are used to coat V_2O_5 films are selected on the basis of their high electrical conductivity, high thermal stability and less corrosiveness as compared to other metals [42].

Current literature focuses very little work on thin film preparation of V_2O_5 by dip coating [43], but no work is found in the literature regarding electrochemical study (e.g., specific capacitance (SC), specific energy density (SE), specific power density (SP) and efficiency (η)) of V_2O_5 thin film electrodes prepared using vanadium pentaoxide by dip coating. Hence in this article, emphasis has been given on the

*Author for correspondence (bjlokhande@yahoo.com)

preparation of vanadium oxide thin film samples (V_2O_5) by dip coating, and varying number of deposition cycles through the precursor solution. Samples are annealed at 773 K and electrochemical characterizations of the prepared samples are investigated in 1 M $NaNO_3$ electrolyte.

2. Experimental

2.1 *Preparation of precursor*

Well-reported melt-quench technique was used for the preparations of vanadium oxide precursor. Typical melt-quench process would start by melting 10 g V_2O_5 (SD Fine Chem) precursor powder in a ceramic crucible and allowing it to stabilize at 1223 K for 30 min (V_2O_5 powder melts at 943–958 K) [43]. The molten form of V_2O_5 powder is then slowly poured into 1000 ml of double-distilled water and stirred for a period of 1 h. By the same preparative process, Darling *et al* [43] got long fibres or ribbons of V_2O_5 with hydrated solution. The resultant solution was dark orange in colour. Prepared solution was filtered by using Wattman filter paper. Filtered sticky solution was then deposited on the substrates by dip coating method. After deposition, the substrates were dried under IR lamp and annealed at 673 K for 3 h.

2.2 *Preparation of dip-coated V_2O_5 thin samples*

Well-cleaned thin SS substrates (no-304), on which V_2O_5 deposition has to be carried out, were used [44]. Initially, 20 ml of the above-prepared vanadium oxide solution was taken in a beaker as a precursor. Then SS substrates were dipped into the precursor solution at the rate of 5 mm s^{-1} and held for 30 s, then removed out from the precursor at the same rate. After that, the samples were dried under IR lamp and annealed at 773 K for 3 h in air. Prepared samples were thereafter submitted to structural, morphological and electrochemical characterizations.

2.3 *Characterization techniques*

The structural and morphological characterizations of the annealed V_2O_5 samples were confirmed from the diffraction pattern obtained using X-ray diffractometer (RigakuD/max 2550V b+18 kW with Cu-Kα 1 = 1.54056 Å), by varying 2θ from 10 to 90° by the step width of 0.2° and scanning electron microscope (SEM; JEOL model JSM-6360). Optical absorption of the deposited samples was observed in the wavelength range 400–900 nm with the help of Shimadzu (UV 3600) spectrophotometer. Weight of the deposited material was measured by weight difference method using 1×10^{-5} high accuracy microbalance (Contact C–84). Computer-controlled Potentiostat (H CH 600D spl. Electrochemical analyzer/workstation) with standard three electrodes cell was used for electrochemical characterization. Electrochemical measurements were made using the data obtained from cyclic voltammetery (CV) of 1 cm^2 surface area of the deposit. The scan rate variation is applied within the potential window −1.2 to 1.2 V in 1 M $NaNO_3$, platinum wire was used as a counter electrode and saturated Ag/AgCl as a reference electrode. The cyclic voltamogram was used to calculate the SC using the relations (1) and (2). The charge–discharge behaviour of the samples was studied using galvanostatic charge–discharge for different current densities applied to the electrode. Multifrequency impedance measurement was carried out in the frequency range 1 MHz to 1 MHz using AC signal of −0.332 V open-circuit potential. Impedance data were fitted with standard data to search an equivalent circuit using Zsimpwin software [45].

3. Results and discussion

3.1 *Structural, morphological and optical studies*

The structural characterization of the prepared sample was performed using X-ray diffraction (XRD) technique. The XRD pattern of V_2O_5 electrode was used to determine the crystal structure, orientation of the planes and grain size. Figure 1 represents the XRD pattern of V_2O_5 sample electrode annealed in air at 773 K for 3 h. XRD pattern shows number of reflections (200), (010), (110), (020), (220), (620), (811) and (103) indicating polycrystalline nature of the deposit. The observed '*d*' values closely match to the standard '*d*' values taken from JCPDS card no. 72-0598 of V_2O_5 exhibiting orthorhombic crystal structure. The standard and observed '2θ' and '*d*' values are tabulated in table 1. Same structure was reported by Wang *et al* [46] by sol–gel method. The crystallite size of V_2O_5 electrode was calculated by using slow scan of XRD. The estimated average crystallite size (D), using Scherer's formula [47], for (010) peak was ∼87.71 nm. This value is analogous to crystallite size reported by Wang *et al* [46].

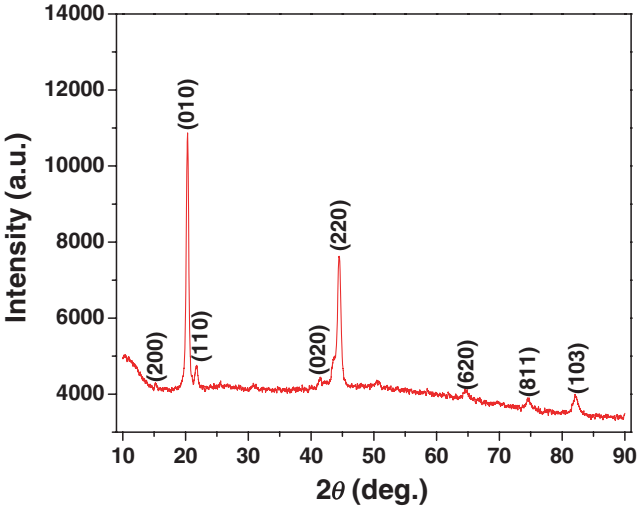

Figure 1. XRD spectra of annealed V_2O_5 sample.

Table 1. Observed and standard '2θ' and 'd' values (matched using JCPDS card no. 72-0598).

Standard '2θ'	Observed '2θ'	Standard 'd'	Observed 'd'	*hkl* Plane
15.42	15.40	5.740	5.791	200
20.35	20.32	4.360	4.366	010
21.78	21.75	4.075	4.080	110
41.38	41.40	2.180	2.177	020
44.41	44.45	2.037	2.034	220
64.77	64.73	1.438	1.438	620
74.75	74.70	1.272	1.271	811
81.74	81.80	1.177	1.172	103

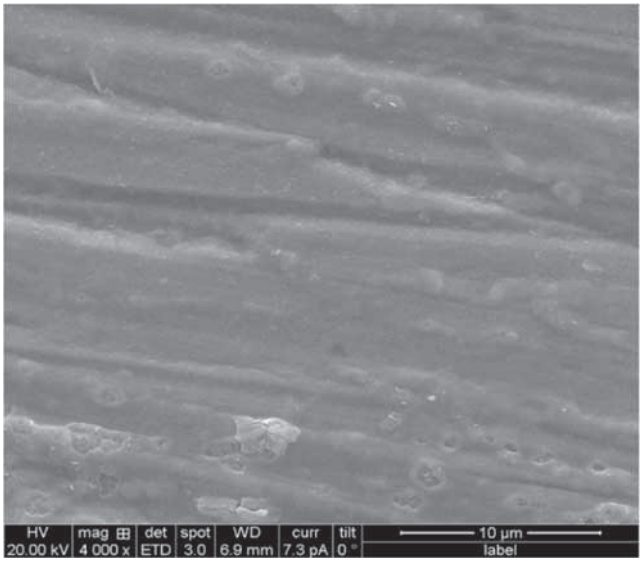

Figure 2. SEM image of annealed V_2O_5 sample.

Surface morphological evaluation of V_2O_5 deposited on to the SS was carried out using SEM digital photo-images. Figure 2 shows the SEM image of annealed sample. Image shows that material is highly dense, uniform and rough in appearance having scratches on the surface. Optical characterization was used to search the bandgap of the material. Figure 3 shows the variation of absorbance (αt) with wavelength λ (nm) for V_2O_5 samples (coated on glass substrates) recorded in the wavelength range 400–1000 nm. The observed value of 'α' is in the order of 10^4. It is further observed that absorption coefficient decreases with increase in wavelength and the sharp cutoff is observed near the band edge reported for CdO by Lokhande and group [48]. This may be attributed to the better crystallinity and lower defect density as observed from XRD. The recorded data were further used to calculate the bandgap energy of the deposited sample using Tauc method [49]. Inset of figure 3 shows the plot of $(\alpha h\nu)^2$ *vs.* $h\nu$. Plot consists of linear portion, which exhibits the presence of direct interband transition in V_2O_5 samples. The obtained bandgap energy for V_2O_5 sample is ~2.25 eV.

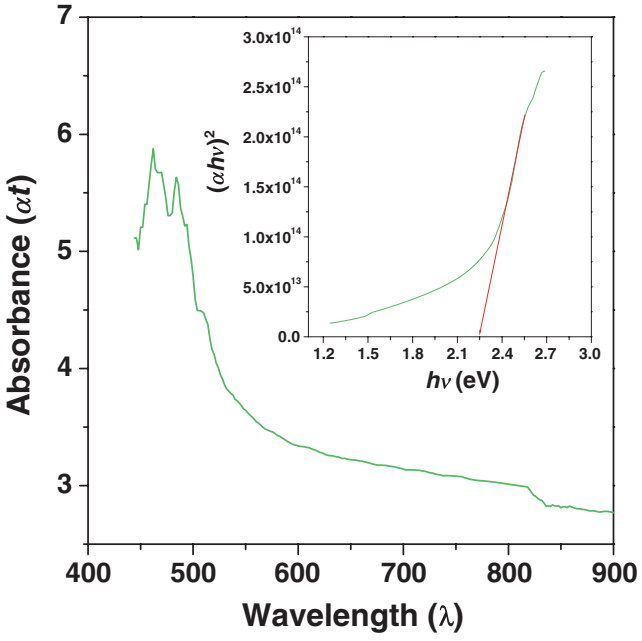

Figure 3. Absorption spectra and inset shows plot of $(\alpha h\nu)^2$ *vs.* $h\nu$.

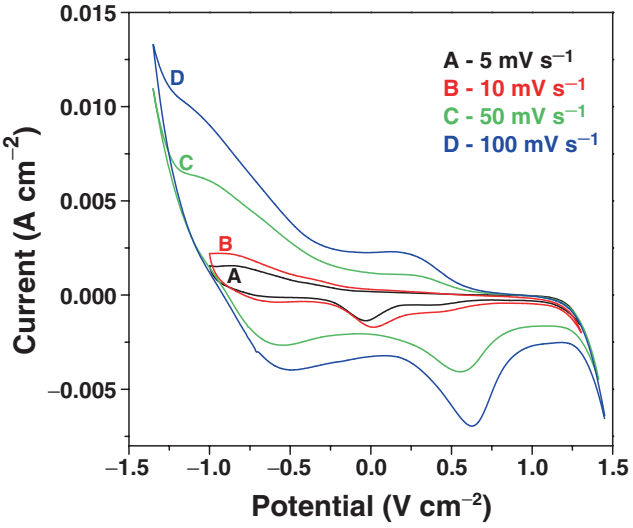

Figure 4. Cyclic voltamograms of annealed V_2O_5 sample at different scan rates.

3.2 *Electrochemical characterization*

Electrochemical behaviour of annealed V_2O_5 sample electrode was observed using CV by varying the scan rate from 5 to 100 mV in 1 M $NaNO_3$ electrolyte. Figure 4 shows the cyclic voltamograms of V_2O_5 sample at different scan rate. It is observed that the shape and area under the CV changes with increase in scan rate. The cyclic voltamogram carried at 5 mV s^{-1} scan rate shows very small area under the curve having single redox peak. With rise in scan rate, area under the peak increases, curve shifts towards negative side of the potential window showing single oxidation peak and two redox peaks. All curves show nearly symmetric behaviour.

By using the following relations [50], the values of SC at different scan rates were evaluated.

$$C = \frac{\int I\,\mathrm{d}t}{\mathrm{d}v/\mathrm{d}t}, \tag{1}$$

$$\mathrm{SC} = \frac{C}{W}, \tag{2}$$

where $\int I\,\mathrm{d}t$ is the area under curve, $\mathrm{d}v/\mathrm{d}t$ the voltage scan rate, C the capacitance and W the weight of the active material dipped in the electrolyte.

Calculated values are tabulated in table 2. It is seen that, the value of SC decreases with increase in scan rate. It shows maximum value of SC, 207.50 F g^{-1}, at lower scan rate 5 mV s^{-1}. The decrease in SC with increase in scan rate has been attributed to the presence of internal vigorous sites that cannot sustain the redox transitions completely at higher scan rates. This is probably due to the improper diffusion of protons within the electrode.

Chronopotentiometric charge–discharge measurement of the annealed V_2O_5 sample electrode was observed at different current densities in 1 M $NaNO_3$ electrolyte. Figure 5 shows charge–discharge variation for annealed V_2O_5 electrode at variable current densities 4–14 mA cm^{-2}. It is observed that with rise in current density, the charge–discharge time decreases and also time variation of potential shifts towards linear nature. At 14 mA cm^{-2}, charge–discharge curve shows maximum symmetric nature indicating good reversible nature of the material at that current density. The electrical parameters such as SE, SP and η were calculated from charge–discharge curves using the following relations [50].

$$\mathrm{SE} = \frac{V \times I\mathrm{d} \times t\mathrm{d}}{W}, \tag{3}$$

$$\mathrm{SP} = \frac{V \times I\mathrm{d}}{W}, \tag{4}$$

$$\eta\% = \frac{t\mathrm{d}}{tc} \times 100, \tag{5}$$

where V is the voltage, Id and td are the discharging current and time (h), W the weight of active electrode (kg and tc the charging time (h).

The calculated values of SE, SP and $\eta\%$ are summarized in table 3, and it is observed that at 14 mA cm^{-2} current density, electrode shows maximum power output.

Electrochemical impedance measurements were made to search internal resistance of the electrode. Figure 6 shows the Nyquist plot between real and imaginary impedance values in the frequency range of 1 mHz–1 MHz, obtained at −0.332 V open-circuit potential. At high frequency region,

Table 2. Variation in SC with scan rate for annealed V_2O_5.

Scan rate (mV s^{-1})	Specific capacitance (F g^{-1})
5	207.50
10	154.38
50	117.38
100	96.56
200	77.56

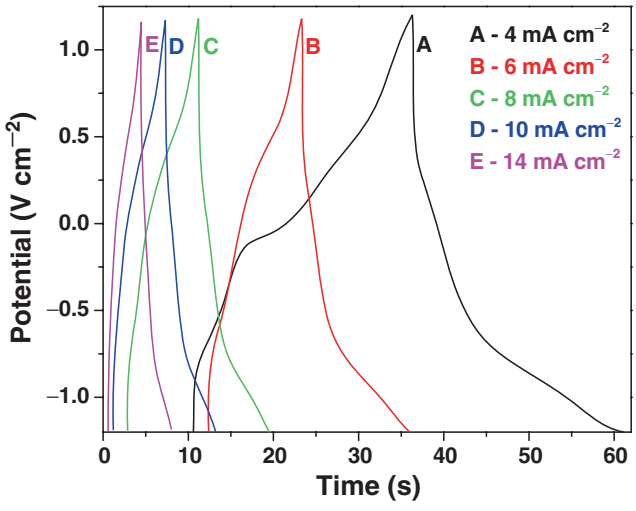

Figure 5. Charge–discharge variation of annealed V_2O_5 sample.

Table 3. Variations of specific energy, specific power and columbic efficiency with applied current densities for annealed V_2O_5 sample.

Current density (mA cm^{-2})	Specific energy (Wh kg^{-1})	Specific power (kW kg^{-1})	Columbic efficiency (%)
04	82.66	12	96.49
06	63.50	18	85.82
08	54.72	24	98.87
10	49.17	30	96.72
14	40.89	42	89.74

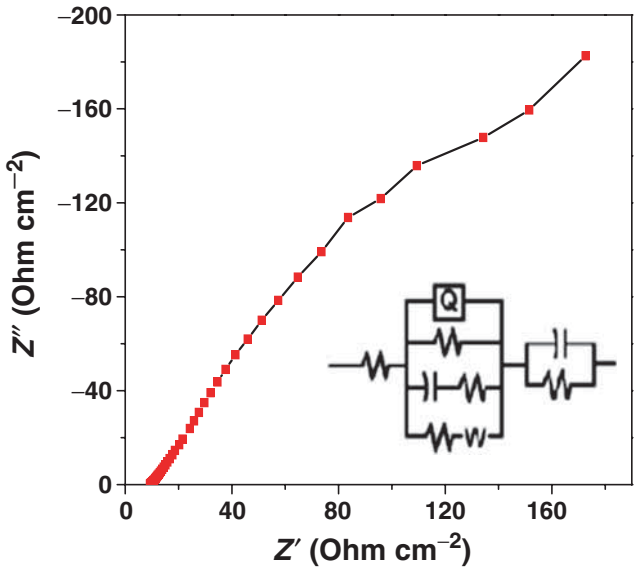

Figure 6. Nyquist plot of annealed V_2O_5 sample and inset shows matched equivalent circuit.

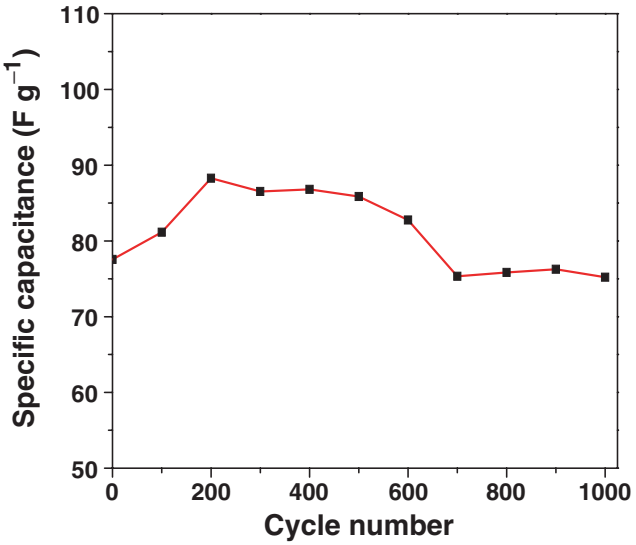

Figure 7. Stability plot of annealed V_2O_5 sample.

the crossover point of the highest frequency with the real part of the impedance is, in general, a combine resistance of the electrolyte, intrinsic resistance of substrate and contact resistance between the active material and the current collector. The observed internal resistance was ∼8.77 Ω cm^{-2}. In the intermediate region of frequency, the straight line nature with the inclination of ∼45° to the real axis was noticed, which is in fact the characteristic of ion diffusion into the electrode materials. In the low frequency range, the straight line part was leaned slowly towards the imaginary axis, indicating that the electrode material experienced capacitive behaviour [50], and inset of it shows matched equivalent circuit obtained by simulation using ZsimpWin software.

Electrochemical stability of V_2O_5 electrode was measured in 1 M $NaNO_3$ at 200 mV s^{-1} high scan rate (figure 7). Here it is observed that with increase in cycle number, the value of SC changes from 77.56 to 88.28 F g^{-1}. Initially it was 77.56 F g^{-1} and increases up to 88.28 F g^{-1} within 200 cycles, later it decreases slowly up to 700 cycles and then remains steady at 75 F g^{-1}. The initial increase in SC was due to complete activation and achievement of optimum condition of the electrode. It also indicates a high degree of reversibility in the repetitive charge–discharge cycles. The later decrease in SC is due to the loss of small amount of active material from the surface of electrode into the electrolyte. Overall, it is observed that material does not show much change in SC with cycle number, indicating good stability of the electrode in repetitive cycling.

4. Conclusions

V_2O_5 thin film electrodes were successfully prepared on SS substrates by a simple dip-coating method via aqueous medium. Deposited V_2O_5 sample shows orthorhombic crystal structure with highly dense and uniform morphology. The optical study proves direct bandgap transition with minimum energy value ∼2.25 eV. The V_2O_5 electrode exhibits a maximum SC of 207.50 F g^{-1} at 5 mV s^{-1}, SE of 82.66 Wh kg^{-1}, SP of 42 kW kg^{-1} and columbic efficiency of 98.87% in 1 M $NaNO_3$ electrolyte. Overall, the study shows that materials have good electrochemical cyclic stability and better capacitive performance.

References

[1] Sarangapani S, Tilak B V and Chen C P 1996 *J. Electrochem. Soc.* **143** 3791
[2] Yan Y, Kim D H, Yang M and Schmuki P 2011 *Chem. Commun.* **47** 7746
[3] Hu C C and Tsou T W 2002 *Electrochem. Commun.* **4** 105
[4] Chen L M, Lai Q Y, Hao Y J, Zhao Y and Ji X Y 2009 *J. Alloys Compd.* **467** 465
[5] Conway B E 1999 *Electrochemical supercapacitors* (New York: Kluwer-Plenum)
[6] Pang S C, Anderson M A and Chapman T W 2000 *J. Electrochem. Soc.* **147** 44
[7] Xia N, Zhou T, Mo S, Zhou S, Zou W and Yuan D 2011 *J. Appl. Electrochem.* **41** 71
[8] Mayer S T, Pekala R W and Kaschmitter J L 1993 *J. Electrochem. Soc.* **140** 446
[9] Prasad K R and Munichandraian N 2002 *J. Electrochem. Soc.* **149** A1393
[10] Mitra S, Shukla A K and Sampath S 2001 *J. Power Sources* **101** 213
[11] Hu C C and Huang Y H 1999 *J. Electrochem. Soc.* **146** 2465
[12] Lokhande C D, Dubal D P and Joo O-S 2011 *Curr. Appl. Phys.* **11** 270
[13] Zheng J P and Jow T R 1995 *J. Electrochem. Soc.* **142** 2699
[14] Hu C C, Huang Y H and Chang K H 2002 *J. Power Sources* **108** 117
[15] Chang C and Chang K H 2000 *Electrochim. Acta* **45** 2685
[16] Cheng F, He C, Shua D, Chen H, Zhang J, Tang S and Finlow E D 2011 *Mater. Chem. Phys.* **131** 268
[17] Qu Q T, Shi Y, Li L L, Guo W L, Wu Y P, Zhang H P, Guan S Y and Holze R 2009 *Electrochem. Commun.* **11** 1325
[18] Lota G, Frackowiak E, Mittal J and Monthioux M 2007 *Chem. Phys. Lett.* **434** 73
[19] Thomberg T, Kurig H, Jänes A and Lust E 2011 *Microporous Mesoporous Mater.* **141** 88
[20] Hua C-C, Huang C-M and Chang K-H 2008 *J. Power Sources* **185** 1594
[21] Si Y C, Jiao L F, Yuan H T, Li H X and Wang Y M 2009 *J. Alloys Compd.* **486** 400
[22] Lee S M, Kim H S and Seong T Y 2011 *J. Alloys Compd.* **509** 3136
[23] Cai C, Guan D S and Wang Y 2011 *J. Alloys Compd.* **509** 909
[24] Wang S Q, Lu Z D, Wang D, Li C G, Chen C H and Yin Y D 2011 *J. Mater. Chem.* **21** 6365
[25] Gu G, Schmid M, Chiu P W, Kozlov M, Munoz E and Baughman R H 2003 *Nat. Mater.* **2** 316
[26] Strelcov E, Lilach Y and Kolmakov A 2009 *Nano Lett.* **9** 2322
[27] Nair H, Gatt J E, Miller J T and Baertsch C D 2011 *J. Catal.* **279** 144
[28] Wu C Z, Wei H, Ning B and Xie Y 2010 *Adv. Mater.* **22** 1972

[29] Lee H Y and Goodenough J B 1999 *J. Solid State Chem.* **148** 81

[30] Li J M, Chang K H and Hu C C 2010 *Electrochem. Commun.* **12** 1800

[31] Chen L M, Lai Q Y, Zeng H M, Hao Y J and Huang J H 2011 *J. Appl. Electrochem.* **41** 299

[32] Wang Y and Cao G 2006 *Chem. Mater.* **18** 2787

[33] Liu Y Y, Clark M, Zhang Q F, Yu D M, Liu D W, Liu J and Cao G Z 2011 *Adv. Energy Mater.* **1** 194

[34] Julien C, Guesdon J P, Gorenstein A, Khelfa A and Ivanov I 1995 *Appl. Surf. Sci.* **90** 389

[35] Ozer N and Lampert C M 1999 *Thin Solid Films* **349** 205

[36] Papaefthimiou S, Leftheriotis G and Yianoulis P 1999 *Thin Solid Films* **343** 183

[37] Capone S, Rella R, Siciliano P and Vasanelli L 1999 *Thin Solid Films* **350** 264

[38] MuthuKaruppasamy K 2008 *Sol. Energy Mater. Sol. Cells* **92** 1322

[39] Patil C E, Tarwal N L, Shinde P S, Deshmukh H P and Patil P S 2009 *J. Phys. D Appl. Phys.* **42** 025404

[40] Borlaf M, Colomer M T, Moreno R and Ortizb A L 2014 *J. Eur. Ceram. Soc.* **34** 4457

[41] Yimsiri P and Mackley M R 2006 *Chem. Eng. Sci.* **61** 3496

[42] Goncalves P R G, Rangel J H G, Oliveira M M, Maciel A P and Longo E 2014 *Ceram. Int.* **40** 12359

[43] Darling R B and Iwanaga S 2009 *Sadhana* **34** 531

[44] Lokhande B J, Ambare R C, Mane R S and Bharadwaj S R 2013 *Mater. Res. Bull.* **48** 2978

[45] Hu C, Yuan S and Hu S 2006 *Electrochim. Acta* **51** 3013

[46] Wang C T and Huang H H 2008 *J. Non-Cryst. Solids* **354** 3336

[47] Cullity B D 1978 *Elements of X-ray diffraction* 2nd edn. (Reading, Massachusetts, USA: Addison-Wesley Publishing Company) Vol. 284

[48] Ambare R C and Lokhande B J 2011 *Inverties J. Renew. Energy* **1** 1

[49] Tauc J, Grigorovici R and Vancu A 1966 *Phys. Status Solidi* **1515** 627

[50] Lokhande B J, Ambare R C, Mane R S and Bharadwaj S R 2013 *Curr. Appl. Phys.* **13** 985